INTERNATIONAL JOURNAL OF
RADIATION ONCOLOGY • BIOLOGY • PHYSICS
www.redjournal.org

PHYSICS CONTRIBUTION

A Predictive Biophysical Model of the Combined Action of Radiation Therapy and Immunotherapy of Cancer

Thomas Friedrich, PhD,* Michael Scholz, PhD,* and Marco Durante, PhD*,†

*Biophysics Department, GSI Helmholtzzentrum für Schwerionenforschung GmbH, Darmstadt, Germany; and †Institute for Condensed Matter Physics, Technical University Darmstadt, Darmstadt, Germany

Received Dec 17, 2021; Accepted for publication Mar 24, 2022

Purpose: Immunotherapy with checkpoint inhibitors has an enormous potential in therapy of metastatic cancers. Immunotherapy is generally combined with local treatments, such as radiation therapy. The time schedule of drug-radiation combination is largely based on empirical observations, and a comprehensive predictive model would be needed to optimize treatments. We present a biophysical model predicting the combined interaction and apply it to describe preclinical experimental data.

Methods and Materials: The model considers the dependences of primary and distal tumor masses, immune cell kinetics targeting tumor cells, and signals causing immune cell replenishment after radiation mechanistic interpretation of the low frequency of abscopal responses. It is benchmarked against 16 experiments with synthetic tumors in murine models.

Results: The model predicts that immune response is stronger for checkpoint inhibitor administration at the time of irradiation or shortly after. The model discriminates correctly between tumor remission and continued growth in all considered experimental cases, including radiation and checkpoint delivery alone or in combination. It identifies a radiation dose window maximizing immune response and avoiding on one side the understimulation of the immune system and radiation-induced depletion of the immune cell pool on the other. Consequently, abscopal effects can be established in certain circumstances only.

Conclusions: The model allows a quantitative mechanistic interpretation of the interaction of radiation with checkpoint blockers and will be helpful for optimizing clinical trials.

Introduction

Combining immune checkpoint blockers with radiation therapy of cancer (called radioimmunotherapy [RIT]) was shown to have the potential to trigger a strong systemic immune response,[1] eventually resulting in abscopal effects.[2,3] The promising results of such combination lead to numerous clinical studies and high expectations in the oncology community.[4] Although benefitting from both systemic effects of immune therapy and targeted radiation action, the combination also exploits the immune stimulating effects of ionizing radiation. Radiation makes cancer cells "visible" to the immune system (ie, overcomes the immune evasion of the cancer), and the combination with immune checkpoint inhibitors (ICIs) has become standard of care within a few years only in certain disease situations.

Corresponding author: Marco Durante, PhD; E-mail: m.durante@gsi.de

Disclosures: none.

Data sharing statement: Research data are stored in an institutional repository and will be shared upon request to the corresponding author.

Supplementary material associated with this article can be found in the online version at doi:10.1016/j.ijrobp.2022.03.030.

Acknowledgments—We thank Dr Alexander Helm for fruitful discussions and thorough proofreading of the manuscript.

https://doi.org/10.1016/j.ijrobp.2022.03.030

Currently, clinical trials using combined ICI-radiation therapy treatment are based on empirical considerations and preclinical experiments in rodents. There, only few combinations of relevant parameters specifying a therapeutic regimen (antibody selection, tumor type, radiation dose and fractionation, scheduling, etc) could be investigated. To describe the underlying mechanisms quantitatively, mathematical models of such multiagent interaction play a key role.

Only a handful of models have been recently published.[5] Practically all theoretical approaches rely on the assumption that ionizing radiation generates "damage signals" or "kill signals" of dying cancer cells initiating an effective antitumor response and reverting the tumor escape from immune surveillance.[6] In RIT, ionizing radiation (IR) generates death-related signals, including different types of damage associated molecular patterns, tumor antigens, and cytokines like interferon beta, leading to a generalized immune response. ICIs regulate T-cell activation and T-cell induced cytolysis of cancer cells, which were suppressed by the tumor before. These connections reflect the cancer immunity cycle[7] with radiation as a trigger for tumor antigen expression. A comprehensive model approach that is applied to various treatment scenarios with a consistent set of model parameters is still lacking. In the present work, we present a predictive model of RIT action based on mechanistic considerations and a limited set of free parameters.

The model describes radiation and the PD-1/CTLA-4 ICI as agents that mediate the interaction among 3 key entities: tumor cells, cytotoxic immune cells (typically lymphocytes), and dying cancer cell signals causing immune cell attraction. In contrast to previous model attempts, it accounts for the dynamics of cell death considering a time distribution of immune response after irradiation, and it will be benchmarked against a broad set of experimental preclinical data taken from the literature.[1,8-16]

Methods and Materials

Model concept

The concept of the derived model is visualized in Figure 1A. It distinguishes between 3 main quantities: tumor cells (tumor mass T), whose inactivation generates attraction signals (signal strength A) such as interferon beta that potentiate the production and attraction of immune cells, resulting in accumulation of typically cytotoxic T-lymphocytes (amount L) in the tumor microenvironment (TME), that finally may inactivate tumor cells. Although different types of immune effector cells and immune signal pathways are known to play distinct self-regulative roles for establishing a well-adjusted immune response, the biologic realm of these is rather abstracted in the model approach, and antitumor immune cells and signals provoking their presence are united in the quantities L and A, respectively. Altogether the mutual dependence of T, A and L is described by the model. With this notation as well as the basic model concept of signal mediated effector cell activation and corresponding constants, we stick to previous model work.[17]

In the model, IR and ICIs modulate interactions between those quantities: radiation enhances the attraction signal level A via tumor cell inactivation. We associate the checkpoint inhibitor aCTLA-4 with fostering the activation of lymphocytes, thus enhancing their presence L in the TME, and aPD-1 (likewise aPD-L1) facilitates their action, reducing tumor cells T. Even if no checkpoint blocker is administered, the model allows the processes of lymphocyte activation and their capability to attack tumor cells by effectively defining base line values of antibodies. The role of radiation in that context is 2-fold. First, radiation inactivates tumor cells but also immune cells in the irradiation field by means of targeted radiation effects. Second, the release of immune cell attracting signals by tumor cell killing reflects the connection between radiation action and immune response.

The tumor and lymphocyte compartments are subdivided corresponding to the primary and the abscopal site (Fig. 1A). For the primary site they are further subdivided in cells unaltered by radiation and moribund cells with lethal radiation damage that leads to inactivation after a delay time. This discrimination is a novel feature of our approach and allows modeling a retarded attraction signal release and a further retarded immune response, as well as a radiation induced loss of lymphocytes as time-continuous processes. Lymphocyte replenishment is considered from the tumor draining lymph nodes and may be inhibited if they lie in the target region. Other compartments relevant for immune cell replenishment like spleen or bone marrow are assumed to lie outside the radiation field.

Mathematical formulation of the model

The interactions between the 3 tumor compartments, the 3 lymphocyte compartments and the amount of attraction signals (Fig. 1A) are described by 7 corresponding retarded differential equations. In cases where only a primary tumor but no abscopal site is considered, the terms corresponding to the latter vanish and a truncated set of 5 equations remains. In the equations, the mutual dependence between the key quantities is modeled by including only basic, effective interaction processes. This turns out to be sufficient to describe the response to RIT adequately.

Retardation comes in as the rate of change of any modelled quantity at time t may depend on that or another quantity at previous times. Practically, the model has been implemented as time discretized difference equations, which have been solved numerically in time steps of 45 minutes. The set of retarded differential equations reads:

$$\dot{T}_1 = \mu_1 T_1 - f_P(L_1 + L_M) - (1 - S_T) \sum_k \delta(\tau_k) T_1 \qquad (1)$$

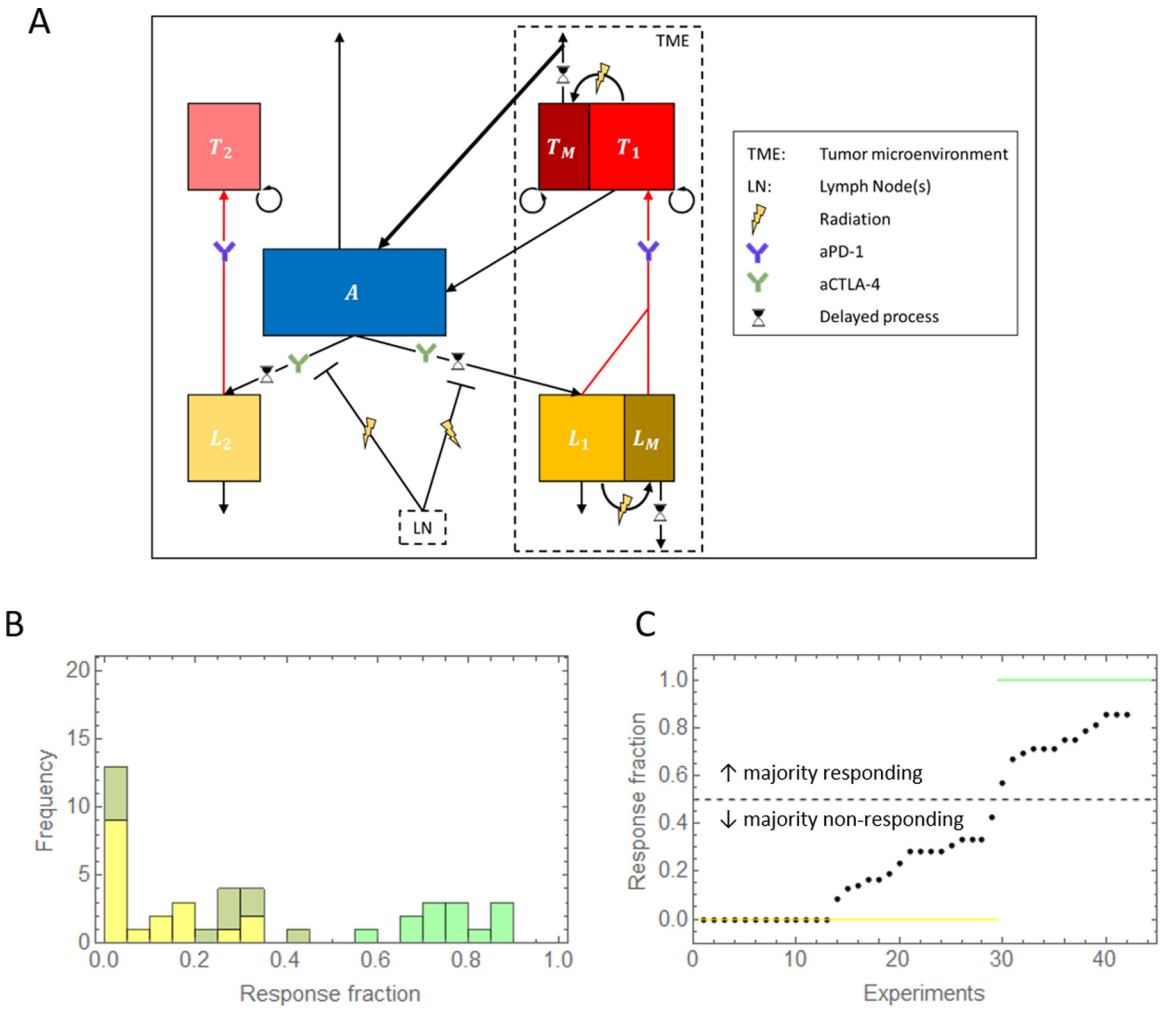

Fig. 1. Model performance. (A) Visualization of the model framework. The interaction of tumor cells T, lymphocytes L, and the amount of immune cell attracting signals A is modulated by therapeutic agents (ie, radiation and antibodies aPD-1 and aCTLA-4). Lymphocytes and tumor cells are subdivided in the tumor microenvironment (index 1) and abscopal site (index 2) and can be converted in the former into moribund cells (index M) by radiation exposure. Moribund tumor cells at first still go on proliferating and finally die out with a delay time distribution (symbolized by the hourglass). Moribund lymphocytes are assumed to continue attacking tumor cells up to that point. While tumor cells proliferate (reflected by the circular arrow), attraction signals and lymphocytes decrease in time, indicated by arrows leading to nowhere. The damage signal release from dying tumor cells increases the level of attraction signals and usually by far compensates the aforementioned loss. In the presence of aCTLA-4 this provokes the replenishment of lymphocytes after another delay, whereby this replenishment is suppressed if lymph nodes are irradiated. Lymphocytes can finally attack the tumor effectively if the PD-1 (likewise the PD-L1) checkpoint is sufficiently inhibited (red arrows). (B) Fraction of individuals who responded to therapy in preclinical experiments for which the model reflects tumor remission after radioimmunotherapy (green), or continued tumor growth after radiation therapy (yellow) and radioimmunotherapy (olive). The scored experimental situation corresponds to either a primary tumor or an abscopal site (not distinguished). (C) Ordered response fractions plotted over a running number of the 42 considered experimental situations. The model predictions of tumor remission (green line) or continued growth (yellow line) correspond consistently to cases where most individuals respond (fraction >0.5) or do not respond (fraction <0.5) to therapy, respectively, in agreement with the experiments.

$$\dot{T}_M = (1-S_T)\sum_k T_1(t_k)e^{\int_{t_k}^{t}\mu_1(t')dt'}(\mu_1 I(\tau_k) - D_K(\tau_k)) + (1-S_T)\sum_k \delta(\tau_k)\ T_1 \quad (2)$$

$$\dot{T}_2 = \mu_2 T_2 - f_P a L_2 \quad (3)$$

$$\dot{A} = \rho(T_1+T_2) - \lambda A + \psi(1-S_T)\sum_k T_1(t_k)e^{\int_{t_k}^{t}\mu_1(t')dt'} D_K(\tau_k) \quad (4)$$

$$\dot{L}_1 = \mu_L L_1 + d - f_P L_1 - (1 - S_L) \sum_k \delta(\tau_k) L_1 \quad (5)$$

$$\dot{L}_M = -f_P L_M + (1 - S_L) \sum_k \delta(\tau_k) L_1 + (1 - S_L) \sum_k L_1(t_k) e^{\mu_L \tau_k} (\mu_L\, I(\tau_k) - D_K(\tau_k) \quad (6)$$

$$\dot{L}_2 = \mu_L\, L_2 + d \quad (7)$$

Here, d abbreviates the replenishment of lymphocytes depending on A, given by

$$d = \int_0^t {S_{LN}}^{n(t')} A(t') f_c(t') D_R(t - t') dt', \quad (8)$$

where $n(t')$ labels the number of fractions up to time t'.

In the equations, the index k labels the radiation fractions, and $\tau_k = t - t_k$ is the time passed since the k^{th} fraction given at time t_k. The Kronecker distribution is labeled by δ. An overview of the involved model constants is given in Table 1.

The functions D_K and D_R are the time delay functions for the release of damage (or kill) signals (index K) and the subsequent lymphocyte recruitment (index R), respectively, and I is an integral function of the former. The functions μ_1 and μ_2 are time dependent growth coefficients for the primary and abscopal tumor, respectively, accounting for a power law instead of an exponential tumor growth. The technical implementation of delay functions and growth parameters is outlined in Appendix E1. Note that in Equations 1 to 7, although not explicitly stated, these functions as well as checkpoint inhibition strengths f_P and f_C depend on time, while the argument (t) is omitted for the sake of readability.

In the following the mathematical model structure is motivated. Implementation details are given in Appendix E1. In Equation 1, the 3 sum terms describe the expansion of primary tumor cells, their predation by lymphocytes and the conversion of irradiated tumor cells to moribund tumor cells by each fraction of radiation in proportion to the inactivation probability, $1 - S_T$. Note that tumor cells are removed by lymphocytes simply in proportion to the presence of the latter. The last term of the sum appears also as second term in Equation 2, enhancing the amount of moribund tumor cells. The first term in Equation 2 describes that the amount of tumor cells that became moribund in the past at time t_k go on proliferating since then, but finally die out with a time delay given by the distribution function D_K. Equation 3 describes the dynamics of abscopal tumor cells expanding at time dependent rate μ_2 and decreasing by lymphocyte attacks, which is attenuated by the constant a, effectively taking into account that the tumor is at some distance and attraction of lymphocytes to the abscopal site may be not that strong as from the primary tumor. Note that in Equations 1 and 3 the lymphocyte action directly scales with the inhibition level of PD-1 or PD-L1, f_P, which denotes the rate of inactivated tumor cells per lymphocyte in the TME. Equation 4 describes the level of attraction signals, being produced at any time at low rate from all tumor cells (first term), diminishing again at rate λ (second term), and being potentiated from damage signals originating from each radiation fraction in the past. The latter signal scales with the amount of cells that became moribund by a previous radiation fraction and are now experiencing with their descendant cells their final inactivation. Proliferating up to this time is reflected by the exponential term, and the probability density of ultimate inactivation by D_K. The process is associated with the factor ψ, which forms the heart of the interaction between radiation and immune response, amplifying the radiation action in the context of immune response. The dynamics of lymphocytes is accounted for in Equation 5, where the first term models the continuous loss of lymphocytes at rate μ_L. This rate is negative to realize a loss mechanism. The convolution integral term d defined in Equation 8 describes the lymphocyte replenishment, calculated from the signal strength A at all previous times which gives rise to lymphocyte activation in proportion to the CTLA-4 inhibition level f_C and cell survival in the lymph nodes up to that time, modulated by the delay time distribution for lymphocyte recruitment after activation D_R. The inhibition strength appears depending on time in Equation 8 as it is enhanced during the time of immunotherapy. Note that Equation 8 also contains radiation effects to the lymph nodes, eventually reducing lymphocyte replenishment by their survival probability S_{LN}. The other terms in Equation 5 model the loss of lymphocytes by predating tumor cells and their radiation induced conversion in moribund lymphocytes. Lymphocyte survival in both the tumor microenvironment and in lymph nodes is calculated from the linear quadratic model for the target dose and a typically lower exposure dose of a fraction p of the target dose, respectively. Lymphocyte kill is further considered in Equation 6 resulting in a conversion into moribund lymphocytes (second term). These are reduced as they further inactivate tumor cells (first term) and may increase and later decrease by further proliferation up to final inactivation (third term). Equation 7 finally describes continuous loss of lymphocytes and their replenishment in abscopal site. This can be interpreted as primed blood lymphocytes, which may infiltrate into the abscopal TME with attenuation a compared with the primary tumor (Equation 3).

Experimental data for model benchmarking

The model was applied to 16 data sets taken from the literature. An overview over experimental conditions is given in Table 2. All experiment specific model parameters are listed in Table E1. The experiments comprise murine models with different synthetic tumors, either one tumor to be

Table 1 Model constants

Quantity	Meaning	Value
Input parameters specifying tumor growth		
a_1, a_2	Tumor growth parameters of primary and secondary tumor (scaling)	Adapted from growth curve without therapy
b_1, b_2	Tumor growth parameters of primary and secondary tumor (exponent)	Adapted from growth curve without therapy
Fixed model constants or functions		
μ_L	Growth coefficient of lymphocytes (negative to simulate net loss)	$-0.15\ d^{-1}$
$\{\alpha, \beta\}$	Linear-quadratic parameters for lymphocyte inactivation in the tumor microenvironment and lymph nodes	$\alpha = 0.2\ Gy^{-1}$ and $\beta = 0.14\ Gy^{-2}$, but minimum survival 0.1%
f_P	Inhibition level of PD-1 (scales tumor cell eradication by lymphocytes per time)	Baseline level: $0.02\ d^{-1}$ Therapy level*: $0.6\ d^{-1}$
f_C	Inhibition level of CTLA-4 (scales lymphocyte replenishment per time)	Baseline level: $0.125\ d^{-1}$ Therapy level: $1.25\ d^{-1}$
ρ	Generation of attraction signals per tumor cells and time	$0.15\ d^{-1}$
λ	Loss rate of attraction signals	$0.15\ d^{-1}$
ψ	Amplification of attraction signals due to damage signals	7
$\{k_1, k_2, k_3\}_K$	Delay function parameters for kill signal release times after exposure, triggering lymphocyte activation	$k_1 =$ Dose [Gy]$\times\ 0.04\ d^{-1}$, (but at least 1/7 and no more than 1/2) $k_2 = 0.2\ d^{-1}$ $k_3 = 2.8$
$\{k_1, k_2, k_3\}_R$	Delay function parameters for lymphocyte recruitment times	$k_1 = 0.5\ d^{-1}$ $k_2 = 0.2\ d^{-1}$ $k_3 = 20$
$T_1(0), T_2(0)$	Starting values for amount of tumor cells	10^5
$L_1(0), L_2(0)$	Starting value for amount of lymphocytes	100
Free model parameters		
S_T	Survival of tumor cells of 1 radiation fraction	Freely adapted
p	Fraction of target dose covering the lymph nodes that drain the primary tumor	Freely adapted
a	Attenuation of lymphocyte infiltration in secondary tumor compared with primary	Freely adapted

* Except in data sets 1 and 2 in Moore et al[16]: Very low concentrations of immune checkpoint inhibitors were given in these experiments, and the therapy level was fixed to a lower value of $0.37\ d^{-1}$.
Quantities and constants used in the set of differential equations and associated definitions are listed with their role in the model framework and the asserted values. The first section describes tumor growth without therapy as model input. The second section displays parameters, which are fixed once or show a fixed dose dependence as indicated. The last section lists the open model parameters that are adapted freely to each data set or at least consistently to data on the same model system from the same publication. The values of these experiment-specific parameters are given in Table E1.

irradiated or additionally an abscopal tumor on the contralateral site. For tumor implantation, murine cell lines CT26 (colon carcinoma), 4T1 (mammary gland), TSA (mammary adenocarcinoma), TUBO (human breast cancer), MC38-OVA or MC38 cells (colon adenocarcinoma), or Lewis lung carcinoma cells were used. Investigated treatment scenarios include no treatment, photon radiation therapy alone, one checkpoint blocker given alone, or the combination of radiation and a checkpoint blocker. Radiation doses and schedules as well as the time course of antibody administration vary as well. Experimental results with doses considerably larger than 15 Gy were not considered, as here the prediction and description of radiation effects alone is not validated. The collection of independent experiments serves as a broad testing ground for the model. Most parameters have been fixed once in adaption to the data. Although radiation action depends on dose, the antibody related parameters could be chosen uniformly (with 1 exception; see Table 1) because the administered concentrations were comparable in the experiments.

Table 2 Data set overview

Data set	Cells	Radiation delivery	Antibody administration	Second tumor
Dovedi et al, 1[8]*	CT26	7 Gy, day 7; 3 × 4 Gy, days 7-9	aPD-L1, days 7-14	No
Dovedi et al, 2[8]*	CT26	5 × 2 Gy, days 7-11	aPD-1, days 7-14	No
Dovedi et al, 3[8]*	CT26	5 × 2 Gy, days 7-11	aPD-1, days 7-14	Yes
Dovedi et al[9]*	CT26	5 × 2 Gy, days 7-11	aPD-L1, days 7-28, days 12-33, or days 18-39	No
Demaria et al, 1[1]	4T1	12 Gy, day 13	aCTLA-4, days 14-22	No
Demaria et al, 2[1]*	4T1	2 × 12 Gy, days 13 and 15	aCTLA-4, days 16-24	No
Vanpouille-Box et al[10]*	TSA	8 Gy, day 12; 3 × 8 Gy, days 12-14	aCTLA-4, days 14-22	Yes
Dewan et al, 1[11]	TSA	5 × 6 Gy, days 12-16; 3 × 8 Gy, days 12-14	aCTLA-4, days 14-22	Yes
Dewan et al, 2[11]	TSA	3 × 8 Gy, days 12-14	aCTLA-4, days 12-20, days 14-22, or days 16-23	Yes
Deng et al[12]	TUBO	12 Gy, day 14	aPD-L1, days 14-25	Yes
Alinezhad et al[13]*	CT26	10 × 3 Gy, days 18-20, 23-25, 27, and 29-31; 2 × 10 Gy, days 18 and 28; 15 Gy, day 18	aPD-L1, days 18-26	No
Marciscano et al[14]*	MC38-OVA	12 Gy, day 11	aPD-1 + aCTLA-4, days 10-16	No
Wei et al[15]*	MC38	8 Gy, day 10	aPD-1, days 11-27 or days 7-25	Yes
Moore et al, 1[16]	MC38	16 Gy, day 14 or day 18	aPD-L1, days 13-20 or days 18-26	No
Moore et al, 2[16]	MC38	2 × 8 Gy, days 14 and 15, days 14 and 18, or days 14 and 24	aPD-L1, days 13-20, days 13-24, or days 13-20 and 23-30	No
Moore et al, 3[16]	LLC	2 × 10 Gy, days 14 and 15, days 14 and 18, or days 14 and 24	aPD-L1, days 12-20, days 12-24, or days 12-20 and 22-30	No

List of 16 data sets of in vivo experiments that were taken from 10 publications and are used for model benchmarking, covering various treatment scenarios. The first column labels the data set according to the publication citation, with a running number distinguishing between multiple data sets included. For the 9 experiments marked with an asterisk (*), the data reported include the number of responders among all individuals at test. The second column shows the cancer cell types used for tumor implantation. The third and fourth columns indicate the radiation dose and drug type, respectively, along with the delivery schedule. Multiple entries refer to compared situations in the respective experiment. If fractionated, radiation doses are given multiple times according to the indicated scheme with 1 fraction at the indicated days after tumor implantation. Checkpoint blockers are administered at discrete times as well but assumed to be effective continuously up to 2 days after the last administration, giving rise to the time intervals given in the fourth column. The last column indicates whether the experiment also investigated the response of an abscopal tumor site.

Results

Quantification of preclinical findings

We applied the model to 16 experiments taken from 10 publications as listed in Table 2. After retrieving tumor growth curve parameters from measurements without therapy, we in total simulated 80 therapeutic growth curves with therapy (17 ICI alone, 28 IR alone, and 35 in combination) for a primary tumor and 26 for a secondary tumor (6 ICI alone, 9 IR alone, 11 ICI + IR). The model distinguished in all cases tumor remission from continued growth correctly (figures E2-E17). For this central finding of the present work, experiments were scored as responding whenever more than 50% of the individuals responded with vanished tumor mass toward end of the observation.

To investigate the dispersion in tumor growth curves of preclinical experiments, we inspected 9 of the 16 experimental sets for which data on the response of individuals were available (marked in Table 2). We determined the response frequency among individuals for 42 therapeutic settings (18 radiation therapy [RT] alone, 24 RIT). Figure 1B and 1C show its distribution in the experiments in comparison to the simulation results. The distribution of responding individuals is bimodal and experiments are well committed to either therapy success or failure. A low fraction of responding individuals <0.5 is observed whenever the simulation predicts continued tumor growth. Likewise, the model suggests tumor control in all cases where a high fraction of responding individuals >0.5 was observed.

Besides treatment outcome the model broadly reflects the shape of observed growth. The adaptable parameters (tumor cell survival S_T, dose fraction of lymph node exposure p and, if applicable, lymphocyte attenuation a in the abscopal site) all lie in expected and plausible ranges. Hence the simulations are based on a set of self-consistent parameters. Only parameters describing the experimental situation had

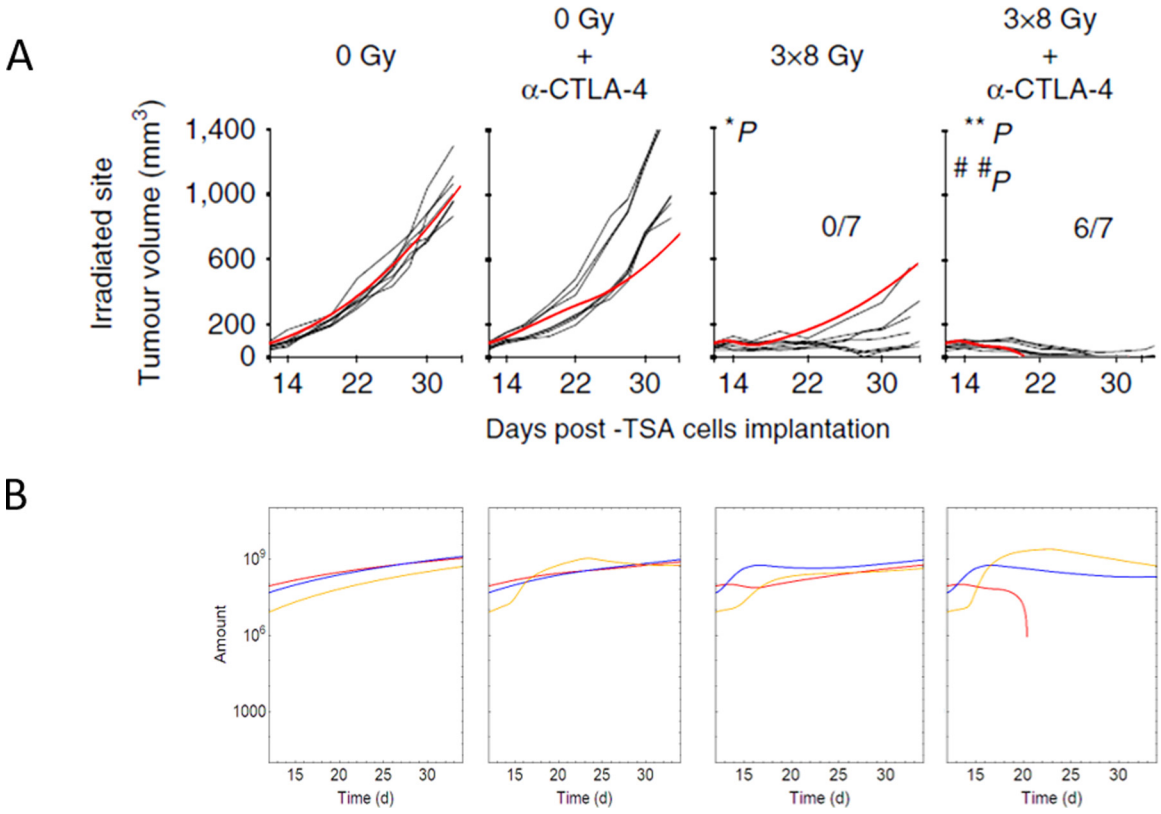

Fig. 2. Primary tumor response. (A) Simulated primary tumor mass (red lines) overlaid to figures published in (10) for different treatment scenarios. Briefly, TSA cells have been implanted in both flanks of BALB/c mice, where we here only consider the primary tumor. Treatment consisted of aCTLA-4 delivery on days 14 to 22 and/or 3 fractions of 8 Gy delivered on days 12, 13, and 14. Note that tumor growth in the original plots in this figure and Figures 3 and 4 is reflected by multiple curves for observed individuals, while the simulation makes point prediction (ie, a single curve). (B) Corresponding simulation results of tumor cells (red), lymphocytes (yellow), and attraction signals (blue). Note that in (A) the quantity T is given as tumor mass (in cubic millimeters) on a linear scale and in (B) as a measure of cell number in logarithmic scale, where 10^6 cells per cubic millimeter are assumed. The quantities L and A are plotted as unnormalized amounts, and a proper normalization is absorbed in the interaction constants. Full data set and model results are displayed in Figure E8.

to be adjusted: tumor growth parameters without therapy as input data, and the 2 (or 3) aforementioned adaptable parameters (Table E1).

Antitumoral lymphocyte activity

In Figure 2 we demonstrate the modeled quantities T, A, and L as a function of time for primary tumor growth data in an experiment presented by Vanpouille-Box et al.[10] In the first days after implantation, where no therapy is administered, T, A, and L reach an equilibrium and increase steadily. Radiation then causes a decrease in tumor mass T and a depletion in the lymphocyte level L soon after irradiation, correlated to survival levels S_T and S_L, respectively. But radiation also enhances the signal level A, which leads to a massive lymphocyte enhancement in case the checkpoint inhibitor aCTLA-4 was administered. The tumor dose response was simulated by means of an adapted tumor cell survival level S_T. Consequently, the tumor mass is effectively reduced in that case, leading to complete remission in the model.

For the simulations the tumor growth curve without therapy is used as model input, and indeed the simulated tumor mass is in agreement with the experimental findings for all considered therapeutic cases (radiation only, aCTLA-4 only, radiation + aCTLA-4). Notably, during treatment time the quantities T, A, and L all vary considerably on the logarithmic scale (ie, over orders of magnitude). Finally, for tumor remission the number of lymphocytes must be available in sufficient concentration compared with the number of tumor cells, and they need to be able to attack the tumor cells as fostered by aPD-1.

Effect of scheduling and field size

Essential for the coherent simulation of radiation and checkpoint inhibitor action is the temporal course of the involved interactions. First, tumor cell inactivation does not take place immediately after irradiation, but is a biologic process

of a certain duration, associated with the delayed elicitation of damage signals, causing a delayed enhancement in the signal level A after exposure. Likewise, T-cell priming, activation and recruitment to the TME give rise to another delay.[18] The presented model includes such delay via temporal distribution terms of interactions. Hence the model is formulated as a set of retarded differential equations.

Figure 3A and 3B demonstrate how the interaction is lost when the PD1 - PD-L1 axis is broken too late after irradiation at hand of data by Dovedi et al.[8] In this case, lymphocytes are accumulated but cannot act against the tumor effectively before checkpoint inhibition starts. If this happens too late, the tumor has grown too big so that despite a high lymphocyte level it is not sufficient to control the tumor. Hence, the model predicts again that failure of therapy is not associated to the amount of effector cells alone (whose action is not prevented from immune checkpoints) but to their number in proportion to tumor size.

Radiation may act systemically in stimulating immune response if tumors are immunogenic,[19] in particular in interaction with immunotherapy.[20] However, this is not its exclusive role, as "classical" targeted radiation affects both tumor cells and immune cells and must be considered as well. The latter process reduces the amount of immune cells and hence may result in immune inhibitory effects of radiation. In particular, this has been demonstrated for the irradiation of regional draining lymph nodes, which is explicitly included in the model. If the lymph nodes are exposed to too high radiation doses, radiosensitive naïve lymphocytes will be inactivated and T-cell activation will be inhibited.

The model includes lymph node exposure by an adaptable proportion factor p of the target dose, so that lymph nodes are exposed to p times the target dose. From that dose the survival level of naïve lymphocytes in the lymph nodes S_{LN} can be calculated, which scales the amount of lymphocytes infiltrating to the TME. As demonstrated in Figure 3C and 3D using data of Marciscano et al,[14] this allows us to describe the response to RIT depending on whether or not the tumor draining lymph nodes lie in the irradiation field. Although the model distinguishes again correctly between tumor remission and continuing growth, the experimental growth curves appear delayed.

Abscopal effects

It is now commonly accepted that the radiation mediated immune response can give rise to abscopal effects, in particular in combination with checkpoint inhibitors. In the presented model the abscopal lesion is simulated in a similar fashion as the primary tumor, and an adaptable parameter a scales the availability of primed lymphocytes with the potential to attack tumor cells at the abscopal site. It was found that this factor is always smaller or equal to 1, therefore motivating its reasonable interpretation as attenuation of lymphocyte availability.

In the model a strong lymphocyte expansion is needed to eradicate both lesions simultaneously. The data set of Wei et al[15] (Fig. 4A) demonstrated that immune therapy, which is given too early will also prevent abscopal tumor rejection. This striking result is reflected in our model, as in that case immunotherapy was terminated earlier in the experiment, providing less time where immune therapy can interact with radiation. In addition, immune cells already accumulated in the TME at the time of irradiation are subject to inactivation and hence cannot effectively contribute to tumor mass eradication.

We observed that abscopal effects are predicted rather rarely for particular situations (ie, specific adjustments of growth parameters, dosage, fractionation, and ICI delivery schedule). To investigate this in more detail, we inspected a hypothetic tumor and an abscopal site and simulated the lesion volume of the latter modulated by RIT with 2 fractions of varying dose and aPD-1 immunotherapy starting at different times. Figure 4B displays the abscopal tumor volume at late times after RIT. Typical values were chosen for all model parameters in this "forward simulation."

It becomes evident that complete remission by RIT may only occur, if at all, in a dose window and for appropriate timing between RT and IT. A small detuning of the schedule may have tremendous effects on treatment outcome. Note that the shown systematics may substantially differ for other tumor growth and radiosensitivity parameters. As a tendency, dose windows get broader for later delivery of immune therapy and are shifted toward smaller doses. This is explained as there is more time to accumulate lymphocytes in that case, whose presence may be stimulated already by small doses, which finally can attack the tumor efficiently when a-PD1 is given.

Discussion

The presented model describes the preclinical data by only using 2 parameters, or 3 when an abscopal tumor is considered. The benefit of the low number of free parameters is that they can be adapted with reasonable uncertainty, and it can be checked that their values are plausible compared with experiments. The cost of including essential processes only is that the complexity of underlying biologic processes is discarded, giving rise to expected model limitations. This tradeoff between model complexity and robustness reflects the general problem of modeling complex systems, where an optimum number of free parameters allows most meaningful model results.[21] This motivates the use of effective parameters. For example, tumor cell survival after irradiation is described by one effective parameter S_T reflecting the average tumor cell survival, and tumor cell heterogeneity or hypoxia would suggest a dispersion in that quantity between different subpopulations.

Previous model approaches demonstrate further possible degrees of freedom, as they include a distinction between radiation induced and immunogenic cell death, multiple

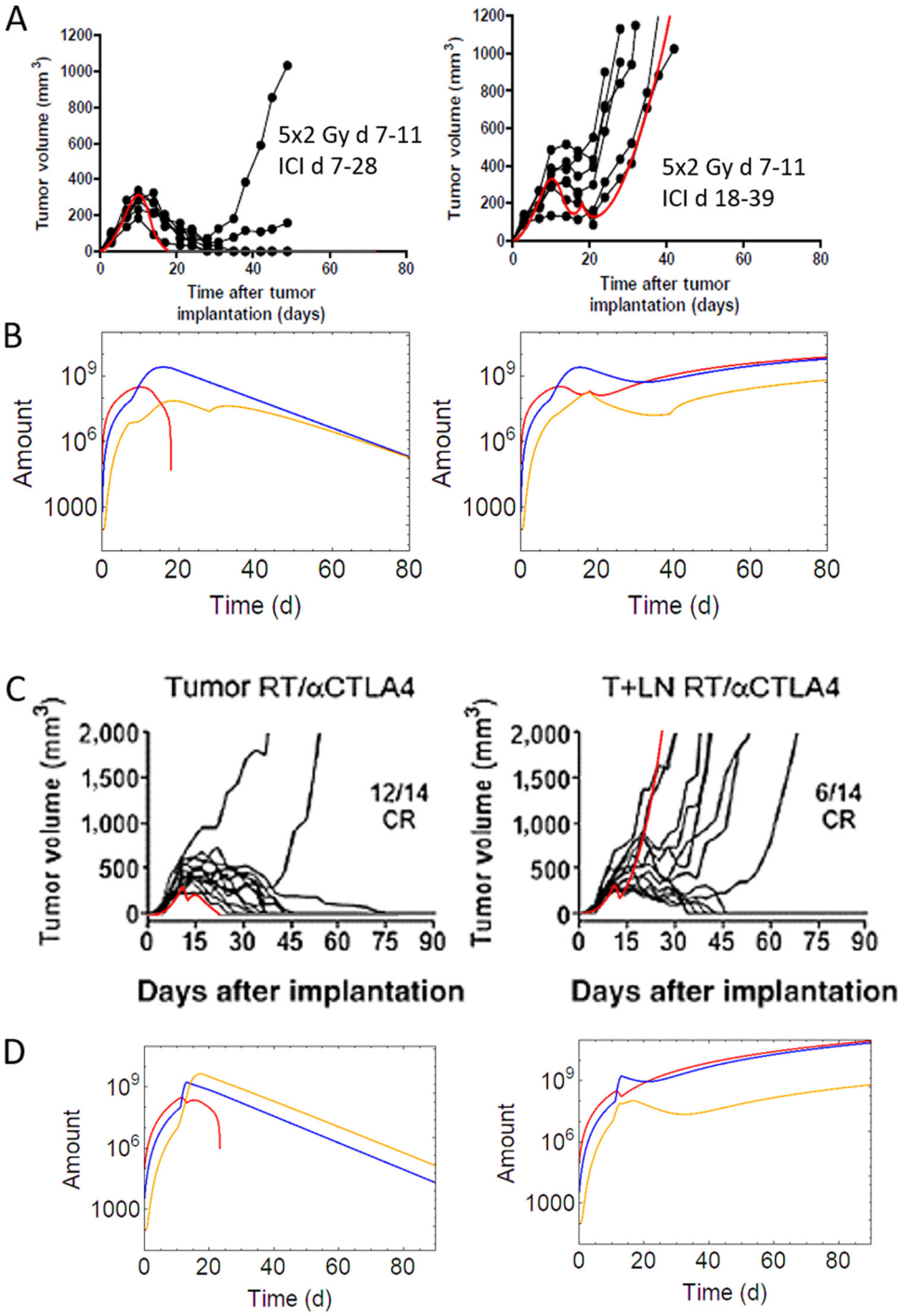

Fig. 3. Effect of scheduling and field size. (A) Simulated tumor mass (red lines) overlaid to figures published in (9) for different relative scheduling of radiation and aPD-L1. Briefly, CT26 cells have been implanted in the flank of BALB/c and C57Bl/6 mice, and treatment consisted of 5 fractions of 2 Gy on days 7 to 11 after implantation, and aPD-L1 delivery on days 7 to 28 or 18 to 39. Full data set and model results are displayed in Figure E5. (B) Simulation results corresponding to (A) of tumor cells (red), lymphocytes (yellow), and attraction signals (blue). (C) Simulated tumor mass (red lines) overlaid to plots originally published in Marciscano et al[14] for radioimmunotherapy with (right) and without (left) lymph node irradiation. MC38-OVA cells have been implanted in the flank of CB57BL/6 mice and treated with 12 Gy on day 11 and aCTLA4 delivery on days 10 to 16. Full data set and model results are displayed in Figure E13. (D) Corresponding model results to the 2 panels in (C), with colors as in previous figures. *Abbreviations:* ICI = immune checkpoint inhibitor; RT = radiation therapy.

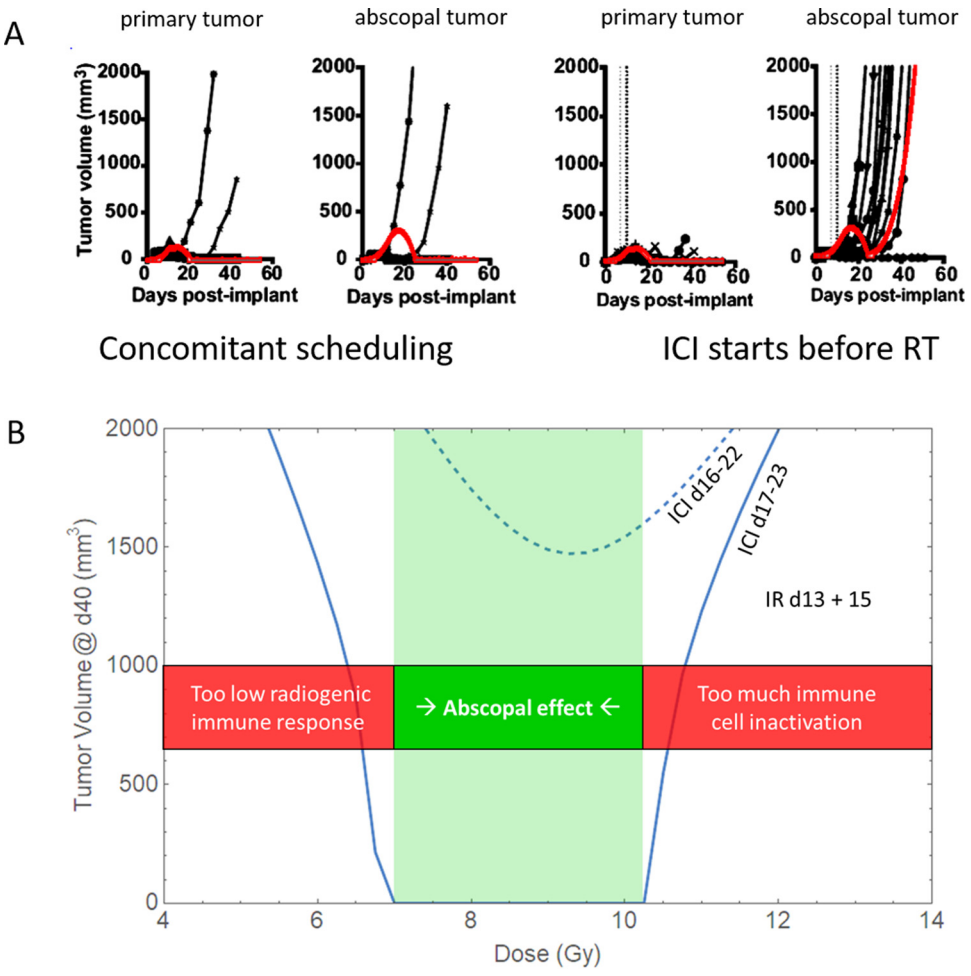

Fig. 4. Abscopal response. (A) Simulated tumor mass (red lines) overlaid to original plots to demonstrate the effects of concomitant and earlier scheduling of immune checkpoint inhibitors compared with radiation for a primary and abscopal tumor in the experiments of Wei et al,[15] where the abscopal response gets lost in the latter case. Full data set and model results are displayed in Figure E14. (B) The simulated abscopal tumor volume on day 40 as a measure of abscopal response is shown in dependence of fraction dose and scheduling. A hypothetic tumor (sensitivity and growth parameters; see Table E1) is irradiated twice (day 13 and day 15), and aPD-1 is enhanced by immunotherapy for 6 days (days 17-23: solid line; days 16-22: dashed line). It was assumed that p = 10% of the target dose covers the tumor-draining lymph nodes, and that lymphocyte recruitment in the abscopal site appears slightly attenuated (a = 0.8) compared with the primary tumor. *Abbreviations:* ICI = immune checkpoint inhibitor; RT = radiation therapy.

differentiation stages of lymphocytes, or the effect of memory cells.[5] In contrast, our model is kept conceptually rather simple to avoid accumulation of free parameters.

Model limits are expected at large doses and at long times. At large doses ($\gtrsim$15 Gy), tumor heterogeneity may lead to an increased survival of the resistant cells compared with sensitive ones,[22] vascular damage may contribute as an additional effect mechanism,[23] and the validity of the linear-quadratic model is not clear.[24,25] At long ($\gtrsim$20 days) postirradiation time, memory effects of the immune system become relevant, but are neglected in our model. Finally, the model is benchmarked at hand of preclinical experiments only. Aiming at translation into a model applicable in the clinical context it must be considered that the relative importance of relevant processes may be different in humans, because the host immune system is a different one, and therapy targets at endogenous tumors rather than synthetic, fast-growing tumors as in the case of experimental systems.

The strength of the presented model is the ability to reproduce the observed entanglement of RT and ICI in combination experiments. This includes both targeted and immunogenic radiation effects, but also the effect of the CTLA-4 level on lymphocyte activation and of the PD-1/PD-L1 level on lymphocyte action. The different immunobiologic functionality and associated timing is readily acknowledged by the model. In fact, it predicts that a combined action of radiation and both ICI leads to a massive systemic antitumor response. This is in line with clinical observations.[26,27] Our model carefully predicts the response of an abscopal, unirradiated tumor, where infiltration of lymphocytes depends on their availability, which was

enhanced by irradiating the primary site. In that regard, further model investigations will consider the irradiation of multiple lesions, which has been shown to be beneficial in clinical settings.[28,29]

From a theoretical perspective a homogeneous dose coverage of the entire lesion sites is not needed to trigger immune response, as has been shown by exploiting the immunogenic action of radiation alone.[19] Hence even a partial volume irradiation of primary tumor and the largest metastatic sites may be sufficient to establish durable systemic antitumor response.

A key feature to describe the time dependent tumor growth pattern is the implementation of the dynamics of the immune system via delay functions. Frey et al[18] report a localized peak of CD8+ cell after day 8 after IR, and Hettich et al[30] found a large lymphocyte-to-tumor cell ratio within day 5 to 10 after hypofractionated RT. However, Zhang et al[31] demonstrated that repeated fractionated irradiation even within that time interval does not stop immune response, indicating that a subpopulation of recruited lymphocytes still survives and maintains to some extent antitumoral response, which is realized in the model by an offset fraction of 0.1% of all lymphocytes that may not be inactivated.

Although the considered preclinical studies indicate that a concomitant or slightly delayed checkpoint blocker administration relative to radiation is favorable, which is in line with the model, another experiment indicates that this is not necessarily the case for aCTLA-4.[32] In fact, it was not possible to reproduce these experimental results with the model, pointing toward potential model limitations and a lack of knowledge about the modes of action of aCTLA-4. However, this particular experiment is not directly comparable with the ones considered in the present study, as a high dose of 20 Gy was used, and aCTLA 4 was only administered once where no constant high antibody level might be reached as assumed in the model. On the other hand, the experiment indicates aCTLA-4 involvement other than facilitating lymphocyte activation, which is included in the model. This highlights the need for further molecular studies unveiling the mechanisms of checkpoint blockers.

The observed dose window structure of abscopal responses (Fig. 4B) can be understood within the model framework as a tradeoff of immune stimulating and immune suppressive radiation action. At low doses, there is no sufficient immune stimulating effect triggered by radiation inflicted damage signals; at very high doses, immune response is strongly initiated, but cannot act because lymphocytes in the tumor microenvironment are massively inactivated by radiation. Here it is important to note that lymphocytes are rather radiosensitive,[33] making the immune system particularly vulnerable at high doses. Within the dose window the recognition of tumor specific antigens by immune cells and an in consequence an effective antitumoral immune response are maximized.

Lymphopenia, often associated with poor prognosis,[34] is a side effect of radiation therapy for large fields and high fraction doses.[35-37] A strategy to widen the dose window for abscopal responses is therefore to restrict high doses to small fields.[35,38] Besides the unavoidable lymphocyte inactivation in the TME, the tumor draining lymph nodes can be regarded as organs at risk, as they are crucial for the replenishment of antigen primed lymphocytes. Indeed, it has been observed that irradiation or resection of tumor draining lymph nodes or inhibition of their functionality reduces immune response.[14,31,39-41] Although in conventional therapy dissection of disease-free nodes aims at mitigating the metastatic potential of the primary tumor, this paradigm might shift toward accepting lymphoid cell exchange but maintaining immune competence. Also, lymphocytes in the blood may be inactivated in large fields, and the entire blood pool reflects an "organ" at risk.[42-45]

Both aspects may play a role in the treatment of head and neck cancers, where combining ICI with RT is associated with numerous challenges[46-48] and lower clinical gain is observed compared with, for example, none-small cell lung cancer. In 2 studies investigating the benefit of RIT for head and neck squamous cell carcinoma,[49,50] no enhanced combination effect has been detected. Among many possible reasons, immune cell depletion can be suspected, as the cervical lymph nodes are typically irradiated electively in addition to the primary tumor.[47] In contrast, while in glioblastoma patients no beneficial effects of combining RT + ICI were detected, histologic findings verified that T-cell response was established but could not be converted into antitumoral effects.[51] Ongoing studies, for example, an attempt to use 2 ICI drugs to overcome the RIT resistance in head and neck squamous cell carcinoma[27] promise further insight in mechanisms and strategies.

In particular for aCTLA-4 in combination randomized clinical trials show a very selective responsiveness of patients, which is in contrast to the preclinical experiments exploited in this study.[52,53] Reasons may be that the host immune system, tumor growth and heterogeneity and length, mass and timescales are different in humans. Consequently, a translation of the modeling work toward clinical applications will require a better mechanistic understanding and a readaption of involved parameters to address these hurdles. Therefore, further randomized clinical trials would be desirable.

Modern radiation therapy techniques may have the potential to improve the responsiveness to the combination of RT and ICI: charged particle therapy with protons or heavy ions reduces the integral dose and allows an efficient sparing of lymph nodes.[36,37,45,54] It can therefore enhance lymphocyte action in RIT, potentially increasing the number of responding patients. To spare lymph nodes and keep target volumes small, also modern approaches like stereotactic body radiation therapy,[55] intraoperative radiation therapy,[56] or partial tumor irradiation[19] have demonstrated to preserve or stimulate immune competence. Spatial fractionated dose delivery[57,58] also seems to trigger a sufficient immune response. Our model could be in principle applied to the aforementioned RT techniques. Once validated, it may be

considered in clinical decision making and implemented in treatment plan optimization.

References

1. Demaria S, Kawashima N, Yang AM, et al. Immune-mediated inhibition of metastases after treatment with local radiation and CTLA-4 blockade in a mouse model of breast cancer. *Clin Cancer Res* 2005;11(2 Pt 1):728–734.
2. Janopaul-Naylor JR, Shen Y, Qian DC, Buchwald ZS. The abscopal effect: A review of pre-clinical and clinical advances. *Int J Mol Sci* 2021;22:11061.
3. Golden EB, Demaria S, Schiff PB, Chachoua A, Formenti SC. An abscopal response to radiation and ipilimumab in a patient with metastatic non-small cell lung cancer. *Cancer Immunol Res* 2013;1:365–372.
4. Pointer KB, Pitroda SP, Weichselbaum RR. Radiotherapy and immunotherapy: Open questions and future strategies. *Trends Cancer* 2022;8:9–20.
5. Friedrich T, Henthorn N, Durante M. Modeling radioimmune response-current status and perspectives. *Front Oncol* 2021;11 647272.
6. Galluzzi L, Vitale I, Warren S, et al. Consensus guidelines for the definition, detection and interpretation of immunogenic cell death. *J Immunother Cancer* 2020;8: e000337.
7. Chen DS, Mellman I. Oncology meets immunology: The cancer-immunity cycle. *Immunity* 2013;39:1–10.
8. Dovedi SJ, Cheadle EJ, Popple AL, et al. Fractionated radiation therapy stimulates antitumor immunity mediated by both resident and infiltrating polyclonal T-cell populations when combined with PD-1 blockade. *Clin Cancer Res* 2017;23:5514–5526.
9. Dovedi SJ, Adlard AL, Lipowska-Bhalla G, et al. Acquired resistance to fractionated radiotherapy can be overcome by concurrent PD-L1 blockade. *Cancer Res* 2014;74:5458–5468.
10. Vanpouille-Box C, Alard A, Aryankalayil MJ, et al. DNA exonuclease Trex1 regulates radiotherapy-induced tumour immunogenicity. *Nat Commun* 2017;8:15618.
11. Dewan MZ, Galloway AE, Kawashima N, et al. Fractionated but not single-dose radiotherapy induces an immune-mediated abscopal effect when combined with anti-CTLA-4 antibody. *Clin Cancer Res* 2009;15:5379–5388.
12. Deng L, Liang H, Burnette B, et al. Irradiation and anti-PD-L1 treatment synergistically promote antitumor immunity in mice. *J Clin Invest* 2014;124:687–695.
13. Alinezhad M, Bakhshandeh M, Rostami E, Alimohamadi R, Mosaffa N, Jalali SA. Synergistic effects of anti-PDL-1 with ablative radiation comparing to other regimens with same biological effect dose based on different immunogenic response. *PLoS One* 2020;15: e0231507.
14. Marciscano AE, Ghasemzadeh A, Nirschl TR, et al. Elective nodal irradiation attenuates the combinatorial efficacy of stereotactic radiation therapy and immunotherapy. *Clin Cancer Res* 2018;24:5058–5071.
15. Wei J, Montalvo-Ortiz W, Yu L, et al. Sequence of αPD-1 relative to local tumor irradiation determines the induction of abscopal antitumor immune responses. *Sci Immunol* 2021;6:eabg0117.
16. Moore C, Hsu CC, Chen WM, et al. Personalized ultrafractionated stereotactic adaptive radiotherapy (PULSAR) in preclinical models enhances single-agent immune checkpoint blockade. *Int J Radiat Oncol Biol Phys* 2021;110:1306–1316.
17. Serre R, Benzekry S, Padovani L, et al. Mathematical modeling of cancer immunotherapy and its synergy with radiotherapy. *Cancer Res* 2016;76:4931–4940.
18. Frey B, Rückert M, Weber J, et al. Hypofractionated irradiation has immune stimulatory potential and induces a timely restricted infiltration of immune cells in colon cancer tumors. *Front Immunol* 2017;8:231.
19. Tubin S, Popper HH, Brcic L. Novel stereotactic body radiation therapy (SBRT)-based partial tumor irradiation targeting hypoxic segment of bulky tumors (SBRT-PATHY): Improvement of the radiotherapy outcome by exploiting the bystander and abscopal effects. *Radiat Oncol* 2019;14:21.
20. Jagodinsky JC, Harari PM, Morris ZS. The promise of combining radiation therapy with immunotherapy. *Int J Radiat Oncol Biol Phys* 2020;108:6–16.
21. van der Schaaf A, Langendijk JA, Fiorino C, Rancati T. Embracing phenomenological approaches to normal tissue complication probability modeling: A question of method. *Int J Radiat Oncol Biol Phys* 2015;91:468–471.
22. Alfonso JCL, Berk L. Modeling the effect of intratumoral heterogeneity of radiosensitivity on tumor response over the course of fractionated radiation therapy. *Radiat Oncol* 2019;14:88.
23. Fuks Z, Kolesnick R. Engaging the vascular component of the tumor response. *Cancer Cell* 2005;8:89–91.
24. Kirkpatrick JP, Brenner DJ, Orton CG. Point/counterpoint. The linear-quadratic model is inappropriate to model high dose per fraction effects in radiosurgery. *Med Phys* 2009;36:3381–3384.
25. Song CW, Terezakis S, Emami B, et al. Indirect cell death and the LQ model in SBRT and SRS. *J Radiosurg SBRT* 2020;7:1–4.
26. Hodi FS, Chiarion-Sileni V, Gonzalez R, et al. Nivolumab plus ipilimumab or nivolumab alone versus ipilimumab alone in advanced melanoma (CheckMate 067): 4-year outcomes of a multicentre, randomised, phase 3 trial. *Lancet Oncol* 2018;19:1480–1492.
27. Hecht M, Eckstein M, Rutzner S, et al. Primary results of the phase II CheckRad-CD8 trial: First-line treatment of locally advanced head and neck squamous cell carcinoma (HNSCC) with double checkpoint blockade and radiotherapy dependent on intratumoral CD8+ T-cell infiltration. *J Clin Oncol* 2021;39(suppl 15):6007.
28. Brooks ED, Chang JY. Time to abandon single-site irradiation for inducing abscopal effects. *Nat Rev Clin Oncol* 2019;16:123–135.
29. Schubert P, Rutzner S, Eckstein M, et al. Prospective evaluation of all-lesion versus single-lesion radiotherapy in combination with PD-1/PD-L1 immune checkpoint inhibitors. *Front Oncol* 2020;10 576643.
30. Hettich M, Lahoti J, Prasad S, Niedermann G. Checkpoint antibodies but not T cell-recruiting diabodies effectively synergize with TIL-inducing γ-irradiation. *Cancer Res* 2016;76:4673–4683.
31. Zhang X, Niedermann G. Abscopal effects with hypofractionated schedules extending into the effector phase of the tumor-specific T-cell response. *Int J Radiat Oncol Biol Phys* 2018;101:63–73.
32. Young KH, Baird JR, Savage T, et al. Optimizing timing of immunotherapy improves control of tumors by hypofractionated radiation therapy. *PLoS One* 2016;11: e0157164.
33. Nakamura N, Kusunoki Y, Akiyama M. Radiosensitivity of CD4 or CD8 positive human T-lymphocytes by an in vitro colony formation assay. *Radiat Res* 1990;123:224–227.
34. Venkatesulu BP, Mallick S, Lin SH, Krishnan S. A systematic review of the influence of radiation-induced lymphopenia on survival outcomes in solid tumors. *Crit Rev Oncol Hematol* 2018;123:42–51.
35. Ellsworth SG. Field size effects on the risk and severity of treatment-induced lymphopenia in patients undergoing radiation therapy for solid tumors. *Adv Radiat Oncol* 2018;3:512–519.
36. Durante M, Formenti S. Harnessing radiation to improve immunotherapy: Better with particles? *Br J Radiol* 2020;93: 20190224.
37. Chen D, Patel RR, Verma V, et al. Interaction between lymphopenia, radiotherapy technique, dosimetry, and survival outcomes in lung cancer patients receiving combined immunotherapy and radiotherapy. *Radiother Oncol* 2020;150:114–120.
38. d'Alesio V, Pacelli R, Durante M, et al. Lymph nodes in the irradiated field influence the yield of radiation-induced chromosomal aberrations in lymphocytes from breast cancer patients. *Int J Radiat Oncol Biol Phys* 2003;57:732–738.
39. Fransen MF, Schoonderwoerd M, Knopf P, et al. Tumor-draining lymph nodes are pivotal in PD-1/PD-L1 checkpoint therapy. *JCI Insight* 2018;3: e124507.
40. Takeshima T, Chamoto K, Wakita D, et al. Local radiation therapy inhibits tumor growth through the generation of tumor-specific CTL: Its potentiation by combination with Th1 cell therapy. *Cancer Res* 2010;70:2697–2706.

41. Nakamura Y, Fujisawa Y, Okiyama N, et al. Surgical damage to the lymphatic system promotes tumor growth via impaired adaptive immune response. *J Dermatol Sci* 2018;90:46–51.
42. Yovino S, Kleinberg L, Grossman SA, Narayanan M, Ford E. The etiology of treatment-related lymphopenia in patients with malignant gliomas: Modeling radiation dose to circulating lymphocytes explains clinical observations and suggests methods of modifying the impact of radiation on immune cells. *Cancer Invest* 2013;31:140–144.
43. Hammi A, Paganetti H, Grassberger C. 4D blood flow model for dose calculation to circulating blood and lymphocytes. *Phys Med Biol* 2020;65: 055008.
44. Jin JY, Mereniuk T, Yalamanchali A, et al. A framework for modeling radiation induced lymphopenia in radiotherapy. *Radiother Oncol* 2020;144:105–113.
45. Ebrahimi S, Lim G, Liu A, et al. Radiation-induced lymphopenia risks of photon versus proton therapy for esophageal cancer patients. *Int J Part Ther* 2021;8:17–27.
46. Plavc G, Jesenko T, Oražem M, Strojan P. Challenges in combining immunotherapy with radiotherapy in recurrent/metastatic head and neck cancer. *Cancers (Basel)* 2020;12:3197.
47. Qian JM, Schoenfeld JD. Radiotherapy and immunotherapy for head and neck cancer: Current evidence and challenges. *Front Oncol* 2021;10: 608772.
48. McBride S, Sherman E, Tsai CJ, et al. Randomized phase II trial of nivolumab with stereotactic body radiotherapy versus nivolumab alone in metastatic head and neck squamous cell carcinoma. *J Clin Oncol* 2021;39:30–37.
49. Lee NY, Ferris RL, Psyrri A, et al. Avelumab plus standard-of-care chemoradiotherapy versus chemoradiotherapy alone in patients with locally advanced squamous cell carcinoma of the head and neck: A randomised, double-blind, placebo-controlled, multicentre, phase 3 trial. *Lancet Oncol* 2021;22:450–462.
50. Bourhis J, Sire C, Tao Y, et al. Pembrolizumab versus cetuximab, concomitant with radiotherapy (RT) in locally advanced head and neck squamous cell carcinoma (LA-HNSCC): Results of the GORTEC 2015-01 "PembroRad" randomized trial. *Ann Oncol* 2020;31:S1168.
51. Chan HY, Choi J, Jackson C, Lim M. Combination immunotherapy strategies for glioblastoma. *J Neurooncol* 2021;151:375–391.
52. Chicas-Sett R, Morales-Orue I, Rodriguez-Abreu D, Lara-Jimenez P. Combining radiotherapy and ipilimumab induces clinically relevant radiation-induced abscopal effects in metastatic melanoma patients: A systematic review. *Clin Transl Radiat Oncol* 2017;9:5–11.
53. Schoenfeld JD, Giobbie-Hurder A, Ranasinghe S, et al. Durvalumab plus tremelimumab alone or in combination with low-dose or hypofractionated radiotherapy in metastatic non-small-cell lung cancer refractory to previous PD(L)-1 therapy: An open-label, multicentre, randomised, phase 2 trial. *Lancet Oncol* 2022;23:279–291.
54. Keisari Y, Kelson I. The Potentiation of anti-tumor immunity by tumor abolition with alpha particles, protons, or carbon ion radiation and its enforcement by combination with immunoadjuvants or inhibitors of immune suppressor cells and checkpoint molecules. *Cells* 2021;10:228.
55. Finkelstein SE, Timmerman R, McBride WH, et al. The confluence of stereotactic ablative radiotherapy and tumor immunology. *Clin Dev Immunol* 2011;2011 439752.
56. Linares-Galiana I, Berenguer-Frances MA, Cañas-Cortés R, et al. Changes in peripheral immune cells after intraoperative radiation therapy in low-risk breast cancer. *J Radiat Res* 2021;62:110–118.
57. Markovsky E, Budhu S, Samstein RM, et al. An antitumor immune response is evoked by partial-volume single-dose radiation in 2 murine models. *Int J Radiat Oncol Biol Phys* 2019;103:697–708.
58. Johnsrud AJ, Jenkins SV, Jamshidi-Parsian A, et al. Evidence for early stage anti-tumor immunity elicited by spatially fractionated radiotherapy-immunotherapy combinations. *Radiat Res* 2020;194: 688–697.